The role of Npc2 in zebrafish embryonic development

Wei-Chia Tseng[1], Ana J. Escauriza[1], Chon-Hwa Tsai-Morris[2], Benjamin Feldman[2], Christopher A. Wassif[1], Forbes D. Porter[1]*

[1]Section on Molecular Dysmorphology, Division of Translational Research, *Eunice Kennedy Shriver* National Institute of Child Health and Human Development, National Institutes of Health, Department of Health and Human Services, Bethesda, MD, USA, 20892.
[2]Zebrafish Core, *Eunice Kennedy Shriver* National Institute of Child Health and Human Development, National Institutes of Health, Department of Health and Human Services, Bethesda, MD, USA, 20892.

Abstract

Niemann-Pick disease (NPC) is a rare fatal neurodegenerative lysosomal storage disease caused by mutations of either *NPC1* or *NPC2*. NPC2 is a soluble lysosomal protein that in coordination with NPC1 is responsible for the efflux of unesterified cholesterol from the lysosome. Mutations of both genes present a similar cellular pathology, characterized by accumulation of unesterified cholesterol and other lipids in the late endosome/lysosome, while reducing cholesterol bioavailability. Here we present our results of a *npc2* null zebrafish model generated by CRISPR/Cas9 gene targeting. Zygotic *npc2*$^{m/m}$ zebrafish from the intercross of *npc2*$^{+/m}$ individuals showed significant unesterified cholesterol accumulation at larval stages. Most *npc2*$^{m/m}$ adults survived but exhibited a 15% reduction in body size compared with *npc2*$^{+/+}$ of the same age. Additionally, zygotic *npc2*$^{m/m}$ adults exhibited motor and balance defects shortly before a premature death. These findings mimic defects found in human and mice, however the phenotype at embryonic stages were milder than expected. We hypothesized that the lack of phenotype in zygotic *npc2*$^{m/m}$ zebrafish was due to the presence of maternal *npc2* mRNA transcripts present in the oocyte at the time of fertilization. To address this issue, we crossed male *npc2*$^{+/m}$ to female *npc2*$^{m/m}$ zebrafish to obtain maternal-zygotic (MZ) *npc2*$^{m/m}$ zebrafish. MZ*npc2*$^{m/m}$ zebrafish exhibited significant developmental defects including absent otolith, abnormal head/brain development, curved/twisted body axis, no circulating blood cells, and usually die by 72 hpf while *npc2*$^{+/m}$ siblings developed normally. Interestingly, these defects have not been previously reported in connection with either defective NPC2 or blockage of intracellular cholesterol trafficking. RNAseq analysis conducted on 30 hpf M*npc2*$^{+/m}$ and MZ*npc2*$^{m/m}$ embryos revealed a significant reduction in *notch3* expression as well as reduction in other downstream genes in the signally pathway such as *hey1* and *her12*. Our result showed that microinjection of a plasmid containing the constitutively active *notch3* intracellular domain at the 1-cell stage could partially rescue the defects found in MZ*npc2*$^{m/m}$ embryos at 30 hpf, suggesting that Notch3 signaling might be involved some aspects of the pathology found in MZ*npc2*$^{m/m}$ zebrafish since Notch3 plays an important role in the development of blood vessels and central nervous system.

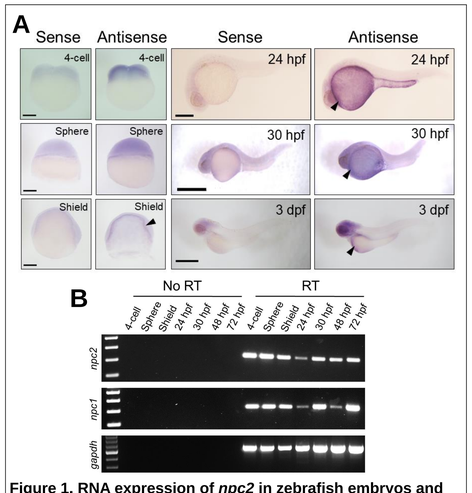

Figure 1. RNA expression of *npc2* in zebrafish embryos and larvae. (A) mRNA expression of *npc2* was shown by *in-situ* hybridization using both sense and antisense probes at various developmental stages. Note the expression was ubiquitous at 4-cell and sphere stage and was more intense in the yolk syncytial layer (arrowhead) at 3 dpf. **(B)** RT-PCR result showed that both *npc2* and *npc1* mRNA was expressed from 4-cell to 72 hpf. *gapdh* was used as an internal control.

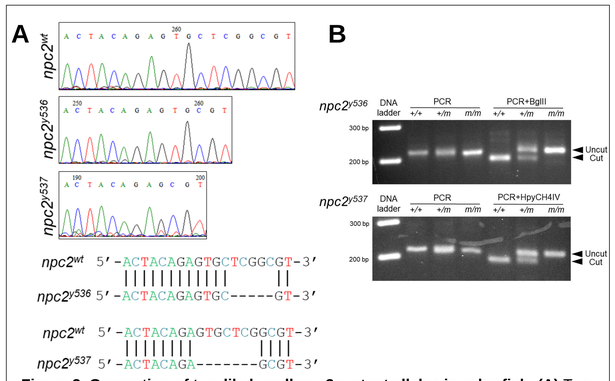

Figure 2. Generation of two likely null *npc2* mutant alleles in zebrafish. (A) Two *npc2* frameshift mutant alleles were identified, namely *npc2*^{y536} *and npc2*^{y537}. **(B)** Genotyping of *npc2* mutants was carried out by using Derived Cleaved Amplified Polymorphic Sequence (dCAPS) primer to introduce an artificial restriction enzyme (RE) sites in PCR products amplified from wildtype *npc2* allele and followed by RE digest. For *npc2*^{y536} allele, PCR product from wildtype but not mutant was expected to be cut by BglII. For *npc2*^{y537} allele, PCR product from wildtype but not *npc2*^{y537} was expected to be cut by HpyCH4IV.

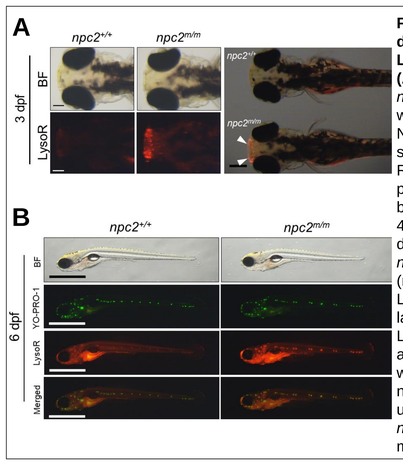

Figure 3. *npc2*$^{m/m}$ larvae displayed intense LysoTracker Red staining. (A) Live 3 dpf *npc2*$^{+/+}$ and *npc2*$^{m/m}$ larvae were stained with LysoTracker Red (LysoR). Note that *npc2*$^{m/m}$ larva showed intense LysoTracker Red staining from olfactory placodes (arrowheads). Scale bar = 100 µm (individual) and 400 µm (overlay). **(B)** Live double staining of *npc2*$^{+/+}$ and *npc2*$^{m/m}$ larvae with YO-PRO-1 (neuromast cell marker) and LysoTracker Red. *npc2*$^{m/m}$ larva exhibited intense LysoTracker Red staining along lateral line neuromasts while the overall pattern of neuromast organization was unaffected comparing with *npc2*$^{+/+}$ larva. Scale Bar = 1 mm.

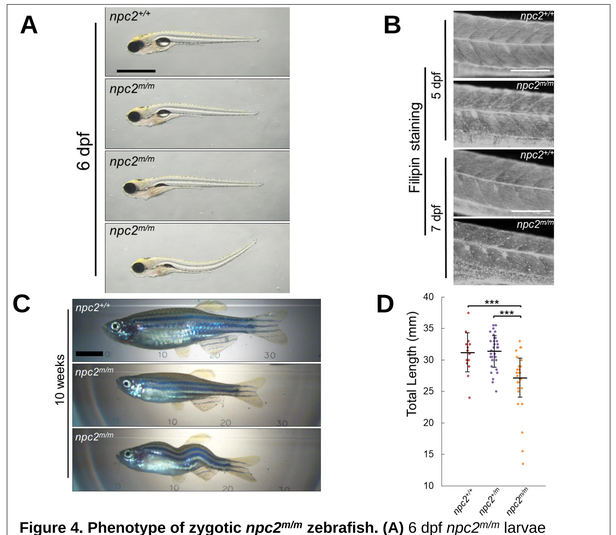

Figure 4. Phenotype of zygotic *npc2*$^{m/m}$ zebrafish. (A) 6 dpf *npc2*$^{m/m}$ larvae exhibited a range of phenotype. Note that *npc2*$^{m/m}$ larvae are mostly identical to *npc2*$^{+/+}$ at this stage. However, few *npc2*$^{m/m}$ larvae displayed the lack of inflated swim bladder and dorsally curved body axis. Scale bar = 1 mm. **(B)** Filipin-positive puncta were found in 5 and 7 dpf *npc2*$^{m/m}$ larvae, indicating the unesterified cholesterol was accumulated in those individuals. Scale bar = 200 µm. **(C)** Live images of 10 wpf *npc2*$^{m/m}$ adults showed relatively normal gross morphology but smaller body size comparing with *npc2*$^{+/+}$ individuals. Nevertheless, some *npc2*$^{m/m}$ adults also showed scoliosis occasionally. Scale bar = 5 mm. **(D)** Total length of *npc2*$^{+/+}$, *npc2*$^{+/m}$, and *npc2*$^{m/m}$ adults at 10 wpf. ***: p<0.001.

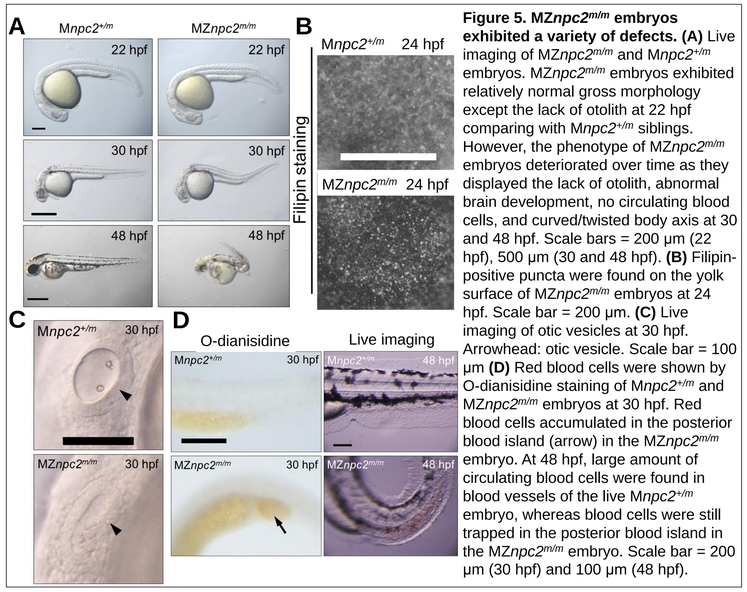

Figure 5. MZ*npc2*$^{m/m}$ embryos exhibited a variety of defects. (A) Live imaging of MZ*npc2*$^{m/m}$ and M*npc2*$^{+/m}$ embryos. MZ*npc2*$^{m/m}$ embryos exhibited relatively normal gross morphology except the lack of otolith at 22 hpf comparing with M*npc2*$^{+/m}$ siblings. However, the phenotype of MZ*npc2*$^{m/m}$ embryos deteriorated over time as they displayed the lack of otolith, abnormal brain development, no circulating blood cells, and curved/twisted body axis at 30 and 48 hpf. Scale bars = 200 µm (22 hpf), 500 µm (30 and 48 hpf). **(B)** Filipin-positive puncta were found on the yolk surface of MZ*npc2*$^{m/m}$ embryos at 24 hpf. Scale bar = 200 µm. **(C)** Live imaging of otic vesicles at 30 hpf. Arrowhead: otic vesicle. Scale bar = 100 µm **(D)** Red blood cells were shown by O-dianisidine staining of M*npc2*$^{+/m}$ and MZ*npc2*$^{m/m}$ embryos at 30 hpf. Red blood cells accumulated in the posterior blood island (arrow) in the MZ*npc2*$^{m/m}$ embryo. At 48 hpf, large amount of circulating blood cells were found in blood vessels of the live M*npc2*$^{+/m}$ embryo, whereas blood cells were still trapped in the posterior blood island in the MZ*npc2*$^{m/m}$ embryo. Scale bar = 200 µm (30 hpf) and 100 µm (48 hpf).

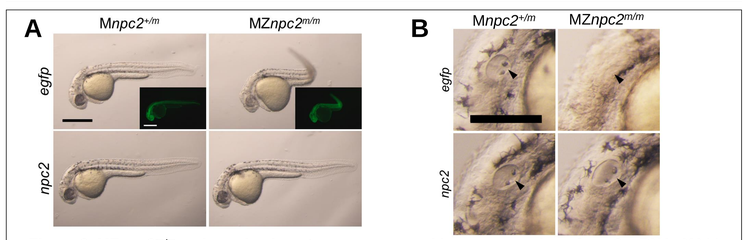

Figure 6. MZ*npc2*$^{m/m}$ embryonic phenotype was rescued by re-expression of *npc2* mRNA. (A) Live imaging of 30 hpf M*npc2*$^{+/m}$ and MZ*npc2*$^{m/m}$ embryos injected with either 50 pg *egfp* or *npc2* mRNA at 1-cell stage. The MZ*npc2*$^{m/m}$ embryo injected with *npc2* mRNA was almost identical to the M*npc2*$^{+/m}$ embryo injected with either *egfp* or *npc2* mRNA, while the MZ*npc2*$^{m/m}$ embryo injected with *egfp* RNA still displayed defects found in uninjected MZ*npc2*$^{m/m}$ embryos. EGFP signal was shown in the insets. Scale bar = 500 µm. **(B)** Zoom-in images of otic vesicles from (A). Note that the otic vesicle and otoliths were normal in the MZ*npc2*$^{m/m}$ embryo injected with *npc2* mRNA (arrowhead). Scale bar = 250 µm.

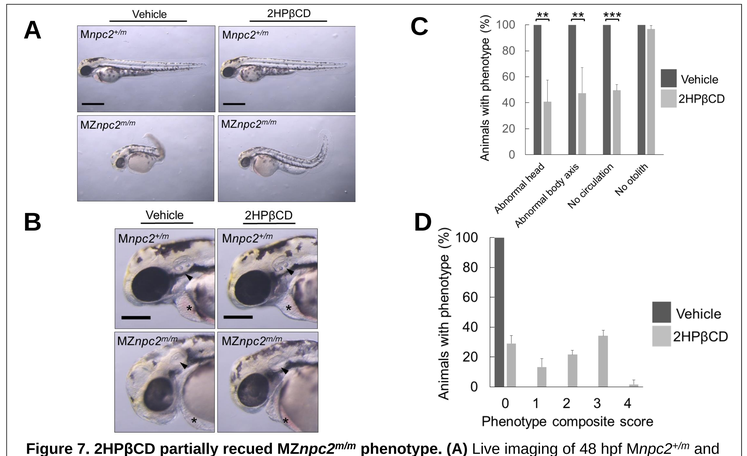

Figure 7. 2HPβCD partially recued MZ*npc2*$^{m/m}$ phenotype. (A) Live imaging of 48 hpf M*npc2*$^{+/m}$ and MZ*npc2*$^{m/m}$ embryos injected with either vehicle or 100 pmol of 2HPβCD at 2.5 hpf. Many 2HPβCD-injected MZ*npc2*$^{m/m}$ embryos showed milder defects such as relatively normal head, restored circulation, and less-curved body axis than those in vehicle-injected MZ*npc2*$^{m/m}$ embryos. Scale bar = 500 µm. **(B)** Zoom-in images from **(A)** showed that although 2HPβCD was able to partially rescue some defects in MZ*npc2*$^{m/m}$ embryos, otoliths were still not seen in MZ*npc2*$^{m/m}$ embryos despite some of them displayed more organized otic vesicles (arrowhead). Note that red blood cells were found in the pericardial region of some 2HPβCD-injected MZ*npc2*$^{m/m}$ embryos but not in vehicle-injected MZ*npc2*$^{m/m}$ embryos (asterisk), suggesting the circulation was restored in those 2HPβCD-injected MZ*npc2*$^{m/m}$ embryos. Scale bar = 200 µm. **(C)** Phenotype of MZ*npc2*$^{m/m}$ embryos was evaluated at 48 hpf. 2HPβCD-injected MZ*npc2*$^{m/m}$ embryos displayed improved phenotype in abnormal head, abnormal body axis, and no circulation while no otolith phenotype was still largely unchanged. **: p<0.01, ***: p<0.001. n=76 (vehicle-injected MZ*npc2*$^{m/m}$ embryos) and n=60 (2HPβCD-injected MZ*npc2*$^{m/m}$ embryos) **(D)** Phenotype composite scores of vehicle and 2HPβCD-treated MZ*npc2*$^{m/m}$ embryos. Individuals exhibited all four defects received a score 0, and individuals with no defect received a score 4. Most 2HPβCD-treated MZ*npc2*$^{m/m}$ embryos had one to three defects improved.

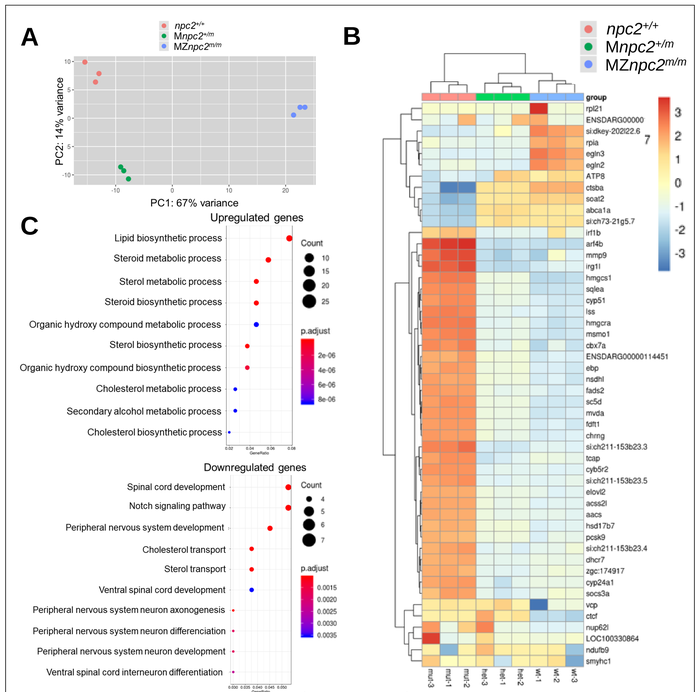

Figure 8. RNA seq analysis of MZ*npc2*$^{m/m}$ and M*npc2*$^{+/m}$ embryos at 30 hpf. (A) Principle component analysis (PCA) of each pool of mRNA from all three genotypes, wildtype (*npc2*$^{+/+}$), heterozygote (M*npc2*$^{+/m}$), and mutant (MZ*npc2*$^{m/m}$). The result suggested that mutant samples varied the most comparing with wildtype and heterozygote samples. **(B)** The heatmap of most varying genes from each pool of mRNA from all three genotypes. The top 50 most-varying genes were selected to compose this heatmap plotting their deviation from the row mean. **(C)** Dotplot of Go biological process analysis of RNA seq result from mutant and heterozygote. This represents top 10 highly enriched GO biological process terms from the analysis with the color corresponding to level of enrichment (adjusted p-value) and the size of the dots representing the number of genes associated with the GO term. The plot represented the up- or down-regulated biological processes in mutant comparing with heterozygote.

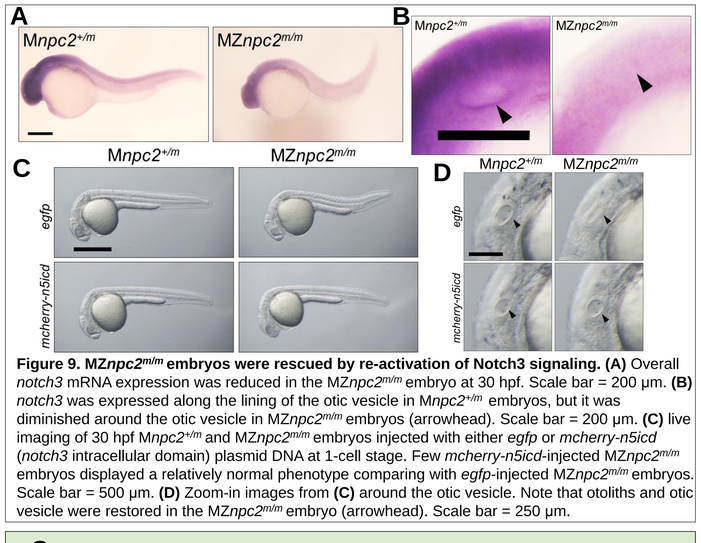

Figure 9. MZ*npc2*$^{m/m}$ embryos were rescued by re-activation of Notch3 signaling. (A) Overall *notch3* mRNA expression was reduced in the MZ*npc2*$^{m/m}$ embryo at 30 hpf. Scale bar = 200 µm. **(B)** *notch3* was expressed along the lining of the otic vesicle in M*npc2*$^{+/m}$ embryos, but it was diminished around the otic vesicle in MZ*npc2*$^{m/m}$ embryos (arrowhead). Scale bar = 200 µm. **(C)** live imaging of 30 hpf M*npc2*$^{+/m}$ and MZ*npc2*$^{m/m}$ embryos injected with either *egfp* or *mcherry-n5icd* (*notch3* intracellular domain) plasmid DNA at 1-cell stage. Few *mcherry-n5icd*-injected MZ*npc2*$^{m/m}$ embryos displayed a relatively normal phenotype comparing with *egfp*-injected MZ*npc2*$^{m/m}$ embryos. Scale bar = 500 µm. **(D)** Zoom-in images from **(C)** around the otic vesicle. Note that otoliths and otic vesicle were restored in the MZ*npc2*$^{m/m}$ embryo (arrowhead). Scale bar = 250 µm.

Summary

- Zebrafish zygotic *npc2* mutants exhibited both early and late defects similar to those found in *npc1* mutants andNPC1 patients.
- MZ*npc2* mutants displayed severe defects at 30 hpf possibly due to the low bioavailability of cholesterol.
- Downregulation of Notch3 signaling might be the cause of most defects found in MZ*npc2* mutants.